FUSION TECHNOLOGY

Annual Report of the Association EURATOM/CEA 2002

Compiled by : Ph. MAGAUD and F. Le VAGUERES

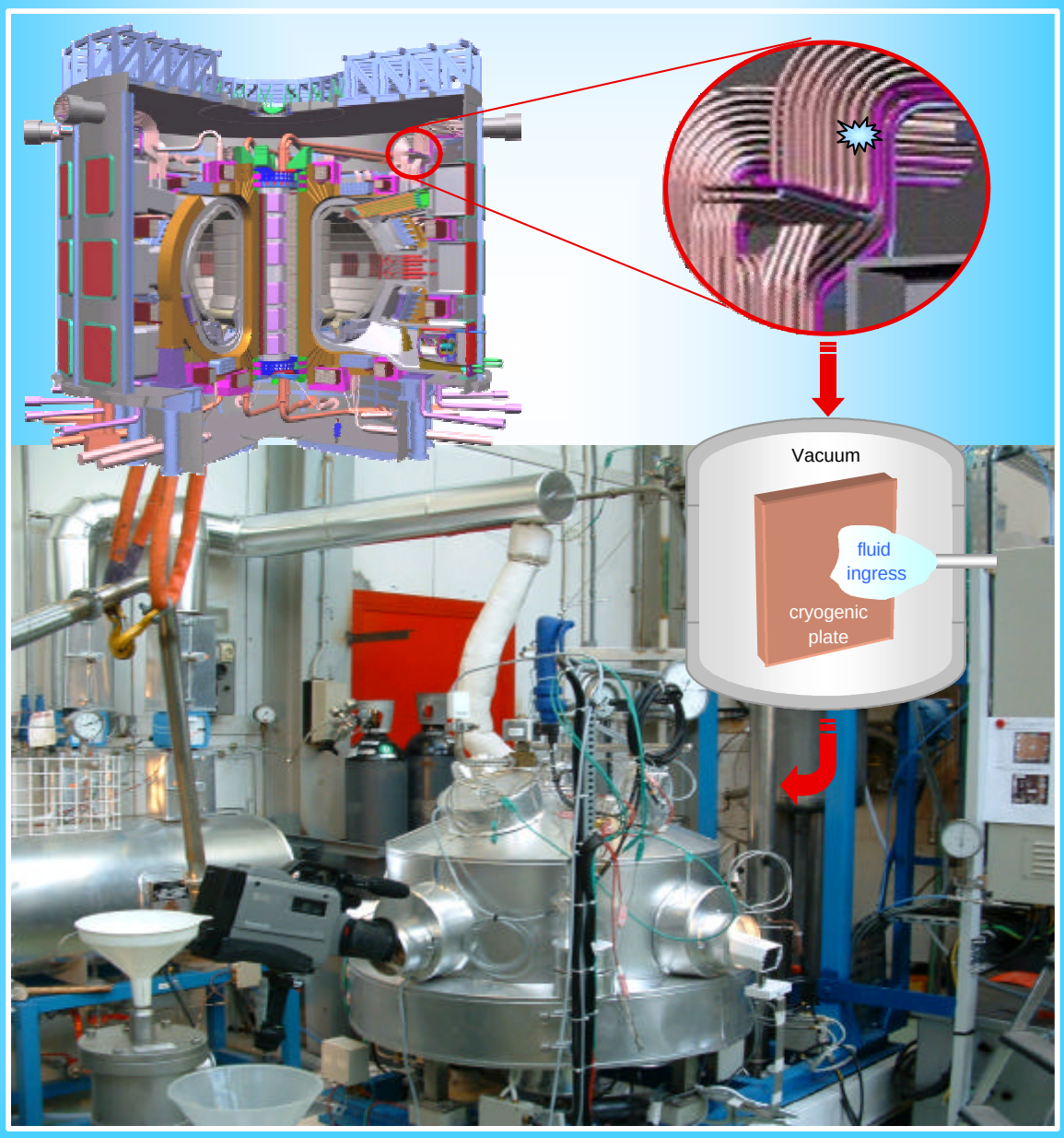

ASSOCIATION EURATOM/CEA
DSM/DRFC
CEA/CADARACHE
13108 Saint-Paul-Lez-Durance (France)

CONTENTS

INTRODUCTION 1

EFDA TECHNOLOGY PROGRAMME 3

Physics Integration

Heating and Current Drive

CEFDA01-645 Support to neutral beam physics and testing 1 5

CEFDA01-646 Support to neutral beam physics and testing 2 9

TW1-TPH-ICRANT ICRF antenna and vacuum transmission line development - Design and manufacturing of a cw ICRF high power test rig and testing of next step antenna prototype components 13

Remote Participation

CEFDA01-647 Support to remote participation in EFDA - RP technical infrastructure assistant 15

TW1-TP/RPINF Development of remote participation infrastructure - Local support to remote participation in the CEA-DRFC 17

Vessel/In-Vessel

Vessel/Blanket

T216-GB8 Small scale testing of FW/BS modules 21

TW0-T420/06 Fabrication of a first wall panel with HIPped beryllium armor 23

TW0-T420/08 Development of HIP fabrication technique 25

TW0-T508/04 Development of Be/CuCrZr HIPping technique 29

TW0-T508/05 Development of Be/CuCrZr brazing technique 31

TW1-TVV-HIP Improvement of HIP fabrication techniques 33

TW1-TVV-LWELD VV intersector joining - Further development of high power Nd-YAG laser welding with multipass filler wire 39

TW1-TVV-ONE Optimisation of one step SS/SS and SS/CuCrZr HIP joints for retainment of CuCrZr properties 43

TW2-TVB-HYDCON Procurement and testing of cutting/welding and inspection tool for the blanket module hydraulic connector 47

TW2-TVV-DISMIT	Evaluation of methods for the mitigation of welding distorsions and residual stresses in thick section welding	51
TW2-TVV-UTINSP	Further development of ultrasonic inspection process	53

Plasma Facing Components

CEFDA99-501	Critical heat flux testing and fatigue testing of CFC monoblocks - 200 kW electron beam gun test	57
CEFDA01-581	Critical heat flux testing of hypervapotrons - 200 kW electron beam gun test	61
CEFDA02-583	Destructive examination of primary first wall panels and mock-ups	65
DV4.3	Optimisation and manufacture of HHF components - Study of flat tile cascade failure possibility for high heat flux components	67
TW0-T438-01	Development and testing of time resolved erosion detecting techniques	71
TW1-TVP-CFC1	Neutron effects on dimensional stability and thermal properties of CFCs	73

Remote Handling

T329-5	In-vessel RH dexterous operations	77
TW0-DTP/1.2 TW0-DTP/1.4 TW1-TVA-IVP TW2-TVR-IVP	In-Vessel Penetrator (IVP) - Prototypical manipulator for access through IVVS penetrations	81
TW1-TVA-BTS	Bore Tool Systems (BTS) - Carrier and bore tools for 4" bent pipes	85
TW1-TVA-MANIP	In-vessel dexterous manipulator	89
TW1-TVA-RADTOL	Radiation tolerance assessment of remote handling components	91

Magnet Structure

CEFDA00-541	Magnet design on PF and correction coils: Conceptual design and analysis	97
M40	Design work on magnet R&D	101
M50	Conductor R&D - Development of NbTi conductors for ITER PF coils	103
TW0-T400-1	CSMC and TFMC installation and test	107
TW1-TMC-CODES	Design and interpretation codes - Determination of thermohydraulic properties of cable-in-conduit conductors with a central channel	109
TW1-TMC-SCABLE	Cable and conductor characterisation - Determination of critical properties and losses of superconducting strands and cables for fusion application	111
TW1-TMS-PFCITE	Poloidal Field Conductor Insert (PFCI)	113
TW2-TMST-TOSKA	TFMC testing with the LCT coil	115

Tritium Breeding and Materials

Breeding Blanket

Water Cooled Lithium Lead (WCLL) blanket

TW1-TTBA-001-D01 TBM adaptation to next step machine 119

TW1-TTBA-001-D03 TBM adaptation to next step machine - Adaptation of mechanical performances to ITER specifications 123

TW2-TTBA-001a-D04 Completion of design activities on WCLL and final report 129

TTBA-2.2 Blanket manufacturing techniques - Solid HIP demonstrator for fabrication and coating 133

TW1-TTBA-002-D05 Blanket manufacturing techniques - Integrated mixed-powder HIP fabrication route for TBM with DWT 137

TW2-TTBA-002a-D02 Crack propagation test and interpretation on unirradiated DWT 141

TW1-TTBA-005-D02 Safety and licensing: Pb-17Li/water interactions 145

Helium Cooled Pebble Bed (HCPB) blanket

TW1-TTBB-002-D02 Blanket manufacturing techniques – Mock-up of FW manufactured with alternative reduced cost fabrication technique 149

TW2-TTBB-002a-D04 Blanket manufacturing techniques - Assessment of first wall fabrication techniques and first wall to stiffening plates joining techniques 151

TW2-TTBB-005a-D03 Development of ceramic breeder pebble beds - Characterization of Li_2TiO_3 pebbles 155

TW2-TTBB-005a-D04 Development of ceramic breeder pebble beds - Mastering and optimising of process parameters for the preparation of Li_2TiO_3 powder and for the fabrication of Li_2TiO_3 pebbles 159

Helium Cooled Lithium Lead (HCLL) blanket

TW2-TTBC-001-D01 Helium-cooled lithium lead - TBM design, integration and analysis - Blanket system design and analysis - Integration and testing in ITER 163

Structural materials development

Reduced Activation Ferritic Martensitic (RAFM) steels

TW1-TTMS-001-D02 RAFM steels - Irradiation performance - TW2-TTMS-001a-D02 Neutron irradiation to 35 dpa at 325°C 167

TW2-TTMS-002a-D04 RAFM steels - Metallurgical and mechanical characterization of Eurofer 97 Thermal ageing behaviour 171

TW2-TTMS-002a-D17 RAFM steels - Tensile and impact test on Eurofer weldments 175

TW2-TTMS-002a-D18 RAFM steels - Tensile and charpy properties of Eurofer powder HIP material 179

TW1-TTMS-003-D12 SCC behaviour of Eurofer 97 in water with additives - Materials compatibility in fusion environments 183

TW2-TTMS-004a-D01 RAFM steels - Eurofer: Powder HIP processing and specification 185

TW2-TTMS-004a-D04 RAFM steels - Eurofer: Fusion welds of structural parts (homogenous welding) 189

TW2-TTMS-004a-D05 RAFM steels - Eurofer: Dissimilar welds development 193

TW2-TTMS-004a-D08 RAFM steels - Powder HIP materials joining 197

TW2-TTMS-004b-D01 RAFM steels - Tubing process qualification: advanced process development and testing for the production of TBM's cooling channels 201

TW2-TTMS-005a-D02 RAFM steels - Rules for design and inspection - DISD appendix A for RAFM steel, intermediate appendix A for the Eurofer steel 205

TW2-TTMS-005a-D05 RAFM steels - Rules for design, fabrication and inspection - Data collection and data base maintenance, update data base for Eurofer steel 209

TW2-TTMS-006a-D01 RAFM steels - ODS processing and qualification 211

TW2-TTMS-006a-D11 TW2-TTMS-006a-D12 ODS/Eurofer HIP joining feasibility solid/solid and solid/powder 215

Advanced materials

TW2-TTMA-001a-D06 Compatibility of SiC_f/SiC with flowing liquid Pb-17Li 219

TW2-TTMA-002a-D04 Feasibility of joining W onto Cu and RAFM steel 223

Neutron source

TTMI-001-D1 IFMIF, accelerator facility - Electron Cyclotron Resonance (ECR) source 225

TTMI-001-D4 IFMIF, accelerator facility - 4 vanes Radio Frequency Quadrupole (RFQ) design 227

TTMI-001-D5 IFMIF, accelerator facility - Radio frequency tube 231

TTMI-001-D6 IFMIF, accelerator facility - Drift Tube Linac (DTL) design 235

TTMI-001-D9 IFMIF, accelerator facility - Diagnostics 239

Safety and Environment

SEA5-31 Validation of computer codes and models 243

TW1-TSS-SEA5 Validation of computer codes and models 245

TW0-SEA3.5 TW1-TSS-SEA3.5 In-vessel hydrogen deflagration/detonation analysis 247

TW1-TSS-SERF2 Tritium releases and long term impacts 249

TW1-TSW-002 Waste and decommissioning strategy 253

System Studies

Power Plant Conceptual Studies (PPCS)

TW1-TRP-PPCS1-D04 Model A (WCLL): Consistency with the PPCS GDRD 255

TW1-TRP-PPCS1-D10 Model A (WCLL): Mechanical analysis design integration 257

TW1-TRP-PPCS5-D03 Environmental assessment: Waste management strategy 261

TW2-TRP-PPCS10-D07 Model D (SCLL): Adaptation of SiC_f/SiC - Pb-17Li divertor concept to the new advanced reactor models 265

TW2-TRP-PPCS11-D01 Model A (WCLL): Study of a high temperature water cooled divertor 269

TW2-TRP-PPCS12-D06 Model D (SCLL): Shield and vacuum vessel design 273

TW2-TRP-PPCS13-D06 Model D (SCLL): Mechanical and thermo-mechanical analysis of the SCLL blanket 277

TW2-TRP-PPCS13-D07 Model D (SCLL) : Design integration (including divertor system) 281

Socio-economic studies

CEFDA01-630 TW1-TRE-FPOA Fusion and the public opinion: Public acceptance of the siting of ITER at Cadarache 287

TW1-TRE-ECFA-D01 Externalities of fusion: Comparison of fusion external costs with advanced nuclear fission reactors 291

TW1-TRE-ECFA-D02 Externalities of fusion accident: Sensitivity analysis on plant model and site location 295

JET Technology

Physics Integration

Diagnostics

CEFDA01-624 Diagnostics enhancement - IR viewing project management and implementation 299

Vessel/In-Vessel

Plasma Facing Components

JET-EP-Div JET EP divertor project 303

JW0-FT-3.1 Internal PFC components behaviour and modelling 305

Remote Handling

CEFDA01-609 Lessons learned from JET maintenance and remote handling operation 307

Safety and Environment

JW0-FT-2.5 Tritium processes and waste management - Dedicated procedures for the detritiation of selected materials 311

UNDERLYING TECHNOLOGY PROGRAMME 315

Physics Integration

Diagnostics

UT-PE-HFW Transparent polycristalline windows 317

Vessel/In-Vessel

Plasma Facing Components

UT-VIV/PFC-TMM Thermo-Mechanical Models (TMM) 321

UT-VIV/PFC-W/Coat Development of thick W CVD coatings for divertor high heat flux components 325

Remote Handling

UT-VIV/AM-Actuators Remote handling techniques - Advanced technologies for high performances actuators 327

UT-VIV/AM-ECIr Remote handling techniques - Radiation tolerance assessment of electronic components from specific industrial technologies for remote handling and process instrumentation 329

UT-VIV/AM-HMI Remote handling techniques - Graphical programming for remote handling techniques 335

UT-VIV/AM-Hydro Remote handling techniques - Technologies and control for remote handling systems 339

Tritium Breeding and Materials

Breeding Blanket

UT-TBM/BB-BNI Blanket neutronic instrumentation 343

UT-TBM/BB-He Helium components technology - Problems and outlines of solutions 347

UT-TBM/MAT-LM/MAG Liquid metal corrosion under magnetic field 349

UT-TBM/MAT-LM/Refrac Compatibility of refractory materials with liquid alloys 353

UT-TBM/MAT-LM/SiC Compatibility of SiC_f/SiC composites with liquid Pb-17Li 357

UT-TBM/MAT-LM/WET Wetting of materials by liquid metals 361

Materials development

Structural materials

UT-TBM/MAT-BIM — Dissimilar diffusion - Bonded joints - Mechanical testing 365

UT-TBM/MAT-HHFC/REFR — Review of refractory metals and alloys for application to high temperature components 369

UT-TBM/MAT-LAM/DES — Design of new reduced activation ferrito-martensitic steels for application at high temperature 371

UT-TBM/MAT-LAM/Mic — Influence of the martensite morphology on the plasticity behaviour of the Eurofer steel 375

UT-TBM/MAT-LAM2 — Irradiated behaviour of Reduced Activation (RA) martensitic steels after neutron irradiation at 325°C 379

UT-TBM/MAT-LAM3 — Microstructural investigation of Reduced Activation Ferritic Martensitic (RAFM) steels and Oxide Dispersion Strengthened (ODS) steels by Small Angle Neutron Scattering (SANS) 383

UT-TBM/MAT-Mod — Modelling of the resistance of the dislocation network to the combined effect of irradiation and stress - Secondary defects structure in an annealed 316L steel after a pulsed and a continuous irradiation - Interaction of pre-existent dislocations and point defects 387

UT-TBM/MAT-ODS — Development of forming and joining technologies for ODS steels 393

Fuel cycle

UT-TBM/FC-SP — Separation of the D/T mixture from helium in fusion reactors using superpermeable membranes - Superpermeable membranes resistant to sputtering - Proposal for superpermeable membrane practical application in fusion 397

Safety and Environment

UT-S&E-LASER/DEC — Laser decontamination: Tritium removal 401

UT-S&E-Mitig — Evaluation and mitigation of the risk connected with air or water ingress 407

System studies

UT-SS-REL — Reliability/availability assessment - Integral approach to assess the availability of the fusion power reactor conceptual designs 409

INERTIAL CONFINEMENT FUSION PROGRAMME 413

ICF01 — Intense laser and particle beams dynamics for ICF applications 415

ICF03 — Laser-matter interaction at relativistic intensities and fast igniter studies 419

ICF04 — EU collaborative experiment on the fast igniter concept 423

ICF-KiT-PRC	Overview on power reactor concepts	425
ICF-XUV-Diag	Dense plasma diagnostics using high order harmonics generation	427

APPENDIX 1 : Directions contribution to the fusion programme 431

APPENDIX 2 : Allocations of tasks 435

APPENDIX 3 : Reports and publications 441

APPENDIX 4 : CEA tasks in alphabetical order 451

APPENDIX 5 : CEA sites 455

ICF01

Task Title: INTENSE LASER AND PARTICLE BEAMS DYNAMICS FOR ICF APPLICATIONS

INTRODUCTION

Our work was devoted (i) to the transport of high current heavy ion beams through plasma, in relation to the Heavy Ion Inertial Fusion (HIIF), and (ii) to the modeling of intense laser and electron beams interacting with plasmas in connection with the fast ignitor concept within the framework of the Inertial Confinement Fusion (ICF) with either laser beams or heavy ion beams drivers. In 2002 we paid special attention to (a) *the numerical simulation of intense ions beams in the target chamber for Heavy Ion Inertial Fusion (HIIF) application,* (b) *experiments on Raman instability, modulated wakefield, and electron acceleration in plasma filled capillary tube* and (c) *first estimate of proton/electron beam efficiency for the hot spot generation in the fast ignitor scenario*. We present below a summary of our results.

2002 ACTIVITIES

(A) FOCUSING IN A HIIF REACTOR

The focusing of the heavy ion beam through several meters inside the reactor chamber is one of the trickiest problems in HIIF. Numerical simulations of target implosion have shown that the focal spot radius of the ion beam should be less than 3 mm. The focusing of several kA over several meters to such a small radius seems not possible under pure ballistic propagation; therefore one has to consider the focusing of the ion beam inside the reactor chamber in the presence of a gas at low or moderate pressure. When the high current beam interacts with the reactor gas two competing processes are appearing. The gas molecules (Flibe) are ionized by the beam. This ionization leads to a screening of the ion-ion interaction among the beam particles. So it tends to reduce the focal spot radius. On the other side, collisions between the projectiles and the gas atoms can ionize the beam ions, thus increasing the ion-ion repulsive force.

To allow for a good propagation, two approaches have been proposed: The first one is to consider a high-pressure gas (above 1 mbar). It leads to a plasma channel type of propagation, where the beam ions are highly ionized. The main problem in this case is to get a well-collimated stable plasma channel. We have considered a second way, at a much lower pressure, the value of the pressure being adjusted to get the optimal screening of the beam. The mean free path for ionization in this scenario is comparable with the radius of the reactor chamber.

The charge state distribution of the beam ions is thus in non-equilibrium, and one has to accurately determine the full collisional-radiative (CR) processes both for the target and for the beam ions. To see the influence of the CR modeling, we have compare two CR calculations. Our results show that in fact the focal spot radius is quite sensitive to the modeling of the collision processes, which should then be accurately determined. To improve the focusing we have also analyze a new concept of beam neutralization using a tube made of isolating material, from which neutralizing electrons can be extracted by the beam, as shown in figure 1.

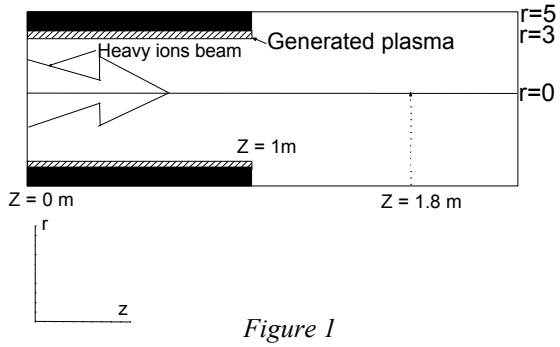

Figure 1

Our results have shown that the focalization is significantly improved by this initial neutralization, as demonstrated in figure 2.

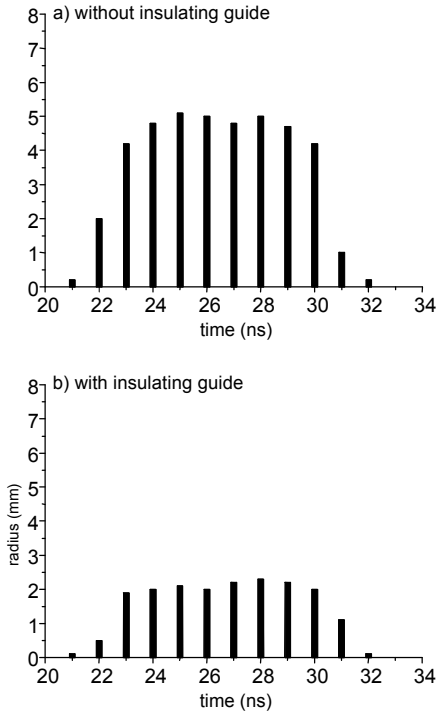

Figure 2 : Beam radius at focus point (Z= 180 cm)

(B) LASER INSTABILITIES IN CAPILLARY TUBES

In the "standard" scenario of the fast ignitor concept, the inner part of the target containing the DT fuel is first compressed to high density by direct or indirect irradiation with megajoule laser or ion beams. Then the ignition of the nuclear reaction is induced in a second step by a short (pico-second) high power electron beam generated by petawatt femto-second laser irradiation.

A high intense laser beam can propagate up to the ultra-dense inner-part of the fusion target, either through a hole created by a first beam, or through a thin empty cone, which is implanted inside the target. In both cases one has to get an accurate knowledge of the propagation of an intense E.M. wave through a target, which has a strong density gradient in the direction transverse to the beam.

The physics related to this particular EM propagation can be best investigated by using well-defined boundary conditions, allowing to clearly identifying the contribution of each parameters. For this we are studying the propagation at the highest intensity presently available of a laser beam through a glass capillary tube either in the void or in the presence of gas. We have simultaneously developed experiment, simulation and analytical treatments in collaboration with several groups. Last year we have presented experimental and theoretical results on the propagation of the E.M. wave.

In 2002 we have addressed the acceleration of electron beams by this E.M. wave. The detection of accelerate electrons allow to diagnose the relative contribution of transverse compare to longitudinal instabilities.

A first experiment have been performed at the terawatt laser beam facilities of the LULI laboratory, to determine whereas acceleration of electrons by wave breaking is possible at low densities, where the relativistic factor ($\gamma_p = \omega_0/\omega_p$) is large, thus allowing to acceleration to high energies. The presence or the absence of accelerated electrons will give a direct signature of longitudinal compare to transverse excitation modes. The experimental results have then been compared with simulation results obtained from the WAKE code (CPht laboratory). The analysis of the wave spectrum has shown Stokes emission, which indicates that Raman instabilities are present, in agreement with the simulation. However no high-energy electrons has been observed.

Following the LULI experiment, another attempt to see high energy electrons produced by laser-plasma interaction at high energy in a capillary tube, have been performed in spring 2002, at the RAL laser facilities, using higher intensities and lower pressures than at the LULI experiment. The results of the experiment are not yet fully analyzed, but the general trends of the LULI experiments seem to occur also for the RAL experiment: High amplitude transverse mode excitations are generated by the laser-plasma interaction. So the wave breaking occurs in the transverse direction, leading to a fast dispersion of the laser beam energy.

These results are of practical importance for the fast ignitor scenario. They show that the transverse dimension is of fundamental importance to predict the beam propagation in the channel at intermediate densities.

In particular for numerical simulation great care has to be put in choosing the boundaries conditions in the transverse direction.

If the transverse dimension of the simulation box is not very large compare to the beam radius (this is the common situation), then periodic conditions do not allow for the dissipation of energy in the transverse direction.

Our experimental work have shown that transverse modes can be the most effective way of damping the incoming energy, thus it has to be correctly taken into account in the simulation of fast ignitor scenario.

(C) PROTON BEAM TRANSPORT

In the "standard" fast-ignitor scenario there are actually two difficult, still unsolved problems: the propagation of the high flux laser beam and the propagation of the generated high current electron beam up to the ultra-high density central domain of the target.

As was discussed in our 2001 reports, instabilities can be quite important for the electron beam, preventing them to reach the central part of the target.

Both for the laser beam and for the electron beam, the situation is highly controversial, so the possibility that the "standard" fast-ignitor scenario can be used is still an open question.

Therefore, it is important to examine whether there exist alternative fast ignitor ways, where non-linear beam-plasma instabilities can be less active. An attractive scheme is to put the laser beam out of the target and to replace the electron beam by a proton one (M. Roth et al. Phys. Rev. Lett., 86, 436, 2001).

Due to their high mass, the protons are much less sensitive to beam-plasma instabilities than electrons, moreover they yield an enhancement of energy deposition at the end of the range (Bragg peak) so that, by adjusting their energy one can deposit the maximum of energy in the right domain.

The interest for using proton beam for the fast ignitor has appearing following very recent experimental results, where high current proton beams with very good emittance properties have been generated by irradiating solid foil with high-power sub-picosecond laser.

We are developing a new simulation code by adapting previous codes devoted to the transport of molecular beams in solid.

This code can be applied to any target (solid, gas, plasma) and include both collision scattering and stopping, and collective effects.

The main ingredients of the simulation code are the following:

(i) The interaction between an ion and the target is described within the dielectric function formalism, using a Mermin form for the dielectric function. The Mermin dielectric function is written as a sum of Random Phase Approximation dielectric function containing adjusted parameters. It allows to reproduce very accurately the collective and binary excitations processes in dense targets, and combines the contribution of both the free and the bound electrons. It has been shown that, for a proton projectile in a solid target, the dielectric function formalism with the Mermin function yields a stopping cross section, which is in agreement with experiment at the 1 % level, for energies from keV up to several MeV.

(ii) A statistical treatment of the interaction process through Monte-Carlo type calculations, which take into account an adjustable distribution for the initial distribution, the dispersion in energy (so-called straggling effect) and ion-ion scattering events, which are calculated using the electronic density of the target ions.

(iii) A dynamical screening (wave effect, see the figures below) between the particles of the beam.

(iv) The description of the travel by the beam from the source, through the target and up to the detector, and a response function of the detector, to allow for a direct comparison with experimental results.

Examples of our results are given in figures 3 and 4, where we have reported the longitudinal and transverse force between two ions of the beam.

The oscillating character of this force comes from the polarization of the plasma electrons. And interesting property of this force is that it is alternatively attractive and repulsive.

So there is a possibility for the ions to be trapped at specific relative distances, yielding to some similarities with cold dusty plasmas, the coupling constant is however much smaller inside the beam than in dusty plasma case.

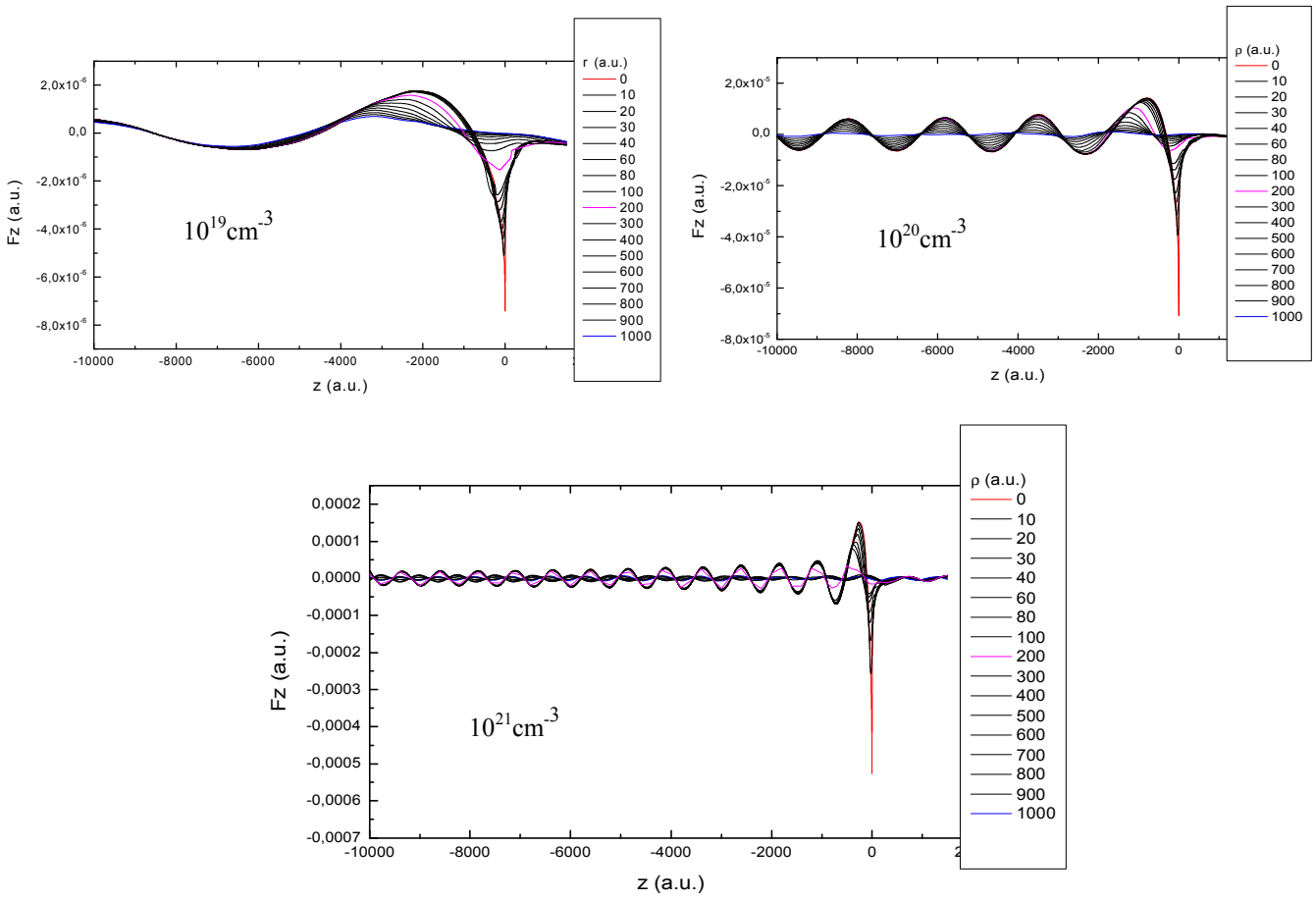

Figure 3 : Wake force induced by a MeV proton
in the longitudinal direction, as a function of the longitudinal coordinate at various transverse distances

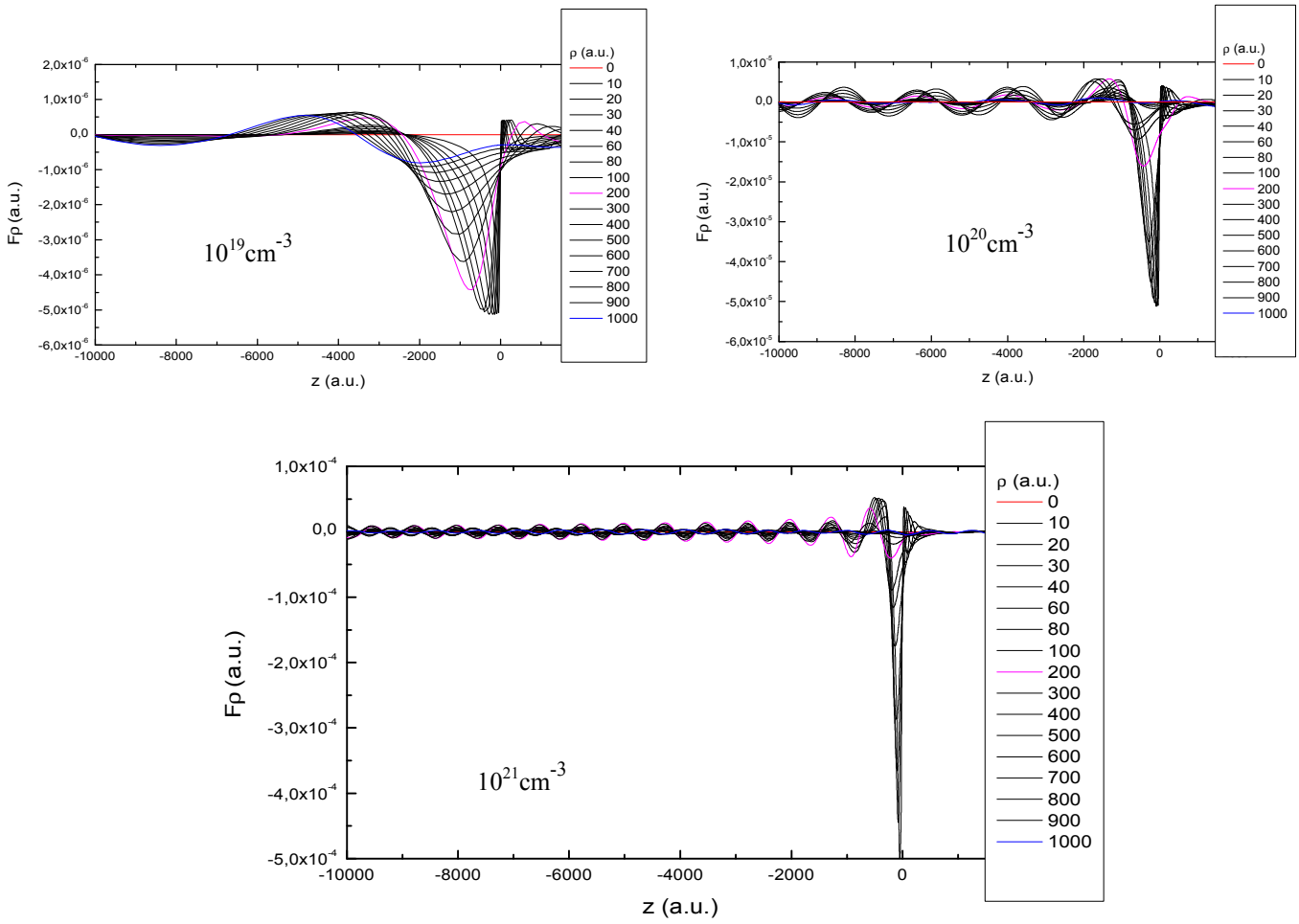

Figure 4 : Wake force induced by a MeV proton in the transverse direction, as a function of the longitudinal coordinate at various transverse distances

REPORTS AND PUBLICATIONS

[P1] Heavy ion-plasma interaction of IFE concern: Where do we stand now? C.Deutsch, H.B. Nersysian, C. Cereceda, Laser and Particle Beams, 20, p1-4 (2002).

[P2] Evaluation of the energy deposition profile for swift heavy ions in dense plasmas G. Maynard, C. Deutsch, K. Dimitriou, K. Katsonis, M. Sarrazin, Nucl. Instrum. Meth. Phys. Res. B 195, 188-215 (2002).

[P3] Quantum and classical stopping cross-sections of swift heavy ions derived from the evolution with time of the Wigner function, G. Maynard, M. Sarrazin, K. Katsonis, K. Dimitriou Nucl. Instrum. Meth. Phys. Res. B 193, 20 (2002).

[P4] Energy loss of MeV/n heavy ions in dense hydrogen plasmas, G. Maynard, C. Deutsch, D. Gardès, M. Chabot, Plasma Sources and Technology 11, A131 (2002).

[P5] Eigen modes for capillary tube with dielectric walls, B. Cros, C. Courtois, G.Matthieussent, A. Di Bernado, D. Batani, N. Andreev, Phys. Rev. E65, 026405 (2002).

[P6] Laser wakefield structure in a plasma column created in capillary tubes, N.E. Andreev, B. Cros, L.M. Gorbunov, G. Matthieussent, P.Mora, R.R. Ramazashvili, Phys. of Plasmas 9, 3999 (2002).

TASK LEADER

Claude DEUTSCH

Laboratoire de Physique des Gaz et des Plasmas
Université Paris XI
Bât. 210
91405 Orsay Cedex

Tél. : 33 1 69 15 76 05
Fax : 33 1 69 15 78 44

E-mail : claude.deutsch@lpgp.u-psud.fr

ICF03

Task Title: LASER-MATTER INTERACTION AT RELATIVISTIC INTENSITIES AND FAST IGNITER STUDIES

INTRODUCTION

The objective of this task was to study, both experimentally and theoretically, the physical mechanisms of laser-matter at relativistic intensities, including laser channelling, electron transport properties beyond the Alfven limit, and the heating by fast electrons with targets having an electron density close or above critical density.

Very promising and new optical diagnostic techniques of relativistic plasma dynamics such as coherent transition radiation and short-pulse laser reflectometry have been studied.

Detailed K-alpha line measurements have been performed to image and characterize quantitatively the electron-heated target core, in conjunction with soft x-ray imaging. Original results in the development of numerical methods for multi-dimensional particle-in-cell simulations have been obtained.

The possibility to perform large-scale simulations, with reduced edge effects, has been particularly emphasized, with over-dense simulations showing hosing instabilities, electron jets formation, and not-so-cold return currents.

Acceleration mechanisms for positively charged particles such as protons have been studied theoretically. Accurate results have been obtained concerning the structure of the ion front, the resultant ion energy spectrum and the maximum ion energy.

2002 ACTIVITIES

EXPERIMENTAL ACTIVITIES

Rear-side optical self-emission from ultra intense laser pulse interactions with solid targets have been used to study electron transport issues. A schematic view of the experimental set-up can be seen in figure 1.

A prompt emission associated with a narrow electron jet has been observed up to aluminium target thicknesses of 400 µm with a 17° typical spreading half-angle.

The quantitative results on the emitted energy are consistent with models where the optical emission is due to transition radiation of electrons reaching the back surface of the target or due to a synchrotron-type radiation of electrons pulled back to the target.

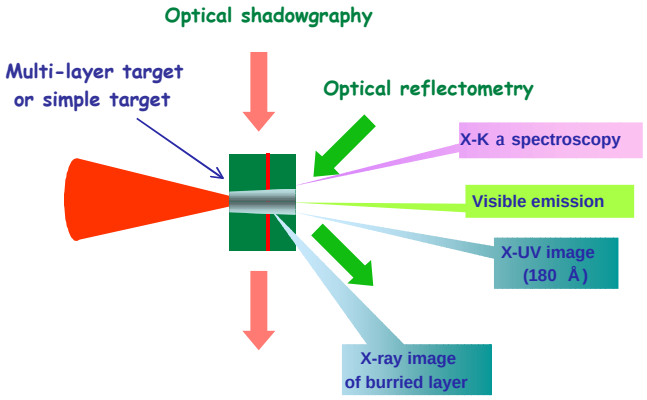

Figure 1 : Schematic view of the experimental set-up showing the various optical diagnostics (shadowgraphy, reflectometry, spectrally resolved visible emission) and the imaging and dispersive (around the K-alpha lines) x-ray diagnostics

Typical time-integrated and time-resolved images are presented in figure 2. On the left, in the time-resolved image of a full energy shot (> 10 J on target) onto a 35 µm thick target, a central narrow bright spot surrounded by a less intense region is observed. On the right is the time-resolved image of a moderate energy shot (~ 5 J on target) onto a 75 µm thick target.

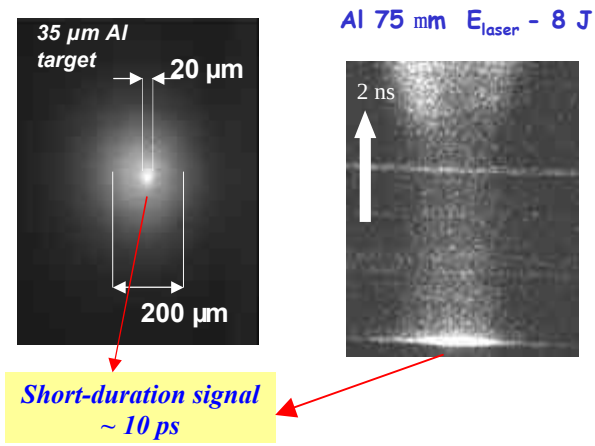

Figure 2 : Time-integrated (left) and time-resolved (right) emission from the rear of the target: the bright, short duration emission at the bottom of the right image lasts approximately 10 ps and corresponds to the bright spot observed on the left spatially resolved image

This result allowed us to distinguish two types of radiation: a first very short duration (less than 10 ps) and very intense signal, followed by a much less intense and long duration signal (of a few ns).

The first one, to which corresponds the bright spot in the integrated image (see figure 2 left), is attributed to fast electrons reaching the target rear surface, whereas the second one is thought to evidence the thermal emission of the cooling and expanding plasma heated by the fast electrons and the associated mechanisms. The signal observed about 4.5 ns after the short signal is interpreted as the breakout of a thermal wave after burning through the target.

A conically bent KDP crystal x-ray spectrometer was used to measure the spectrum between 7 Å and 8.5 Å. This domain includes the cold Al K-alpha line as well as the shifted K-alpha line of heated and ionized Al.

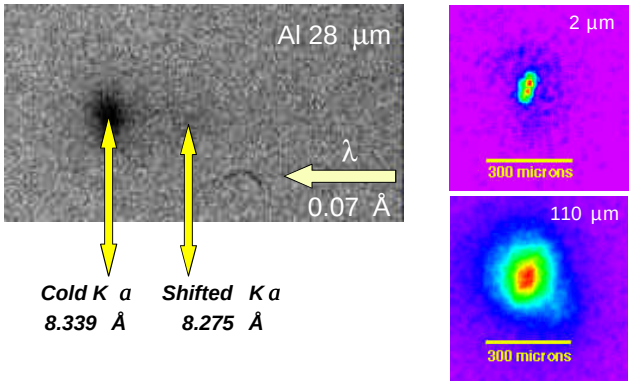

Figure 3 : Spectrum for a 28 µm thick Al target (left, showing cold K-alpha line at 8.339 Å and ionized K-alpha line at 8.275 Å) and Ti K-alpha pictures (right) for a 2 µm thick Ti target (top) and a sandwich target with 110 µm of Al in the front (bottom)

A typical spectrum is shown in figure 3 (left) for a 28 µm thick Al target and incident laser energy of 10 joules. It shows a broad cold K-alpha emission spot (at 8.339 Å) and a shifted K-alpha line at 8.275 Å. This K-alpha line is relatively weak and is only visible up to 50 µm thick targets.

The shift corresponds to an ionization stage (Z*) of 5. From a local thermodynamic equilibrium, the estimated temperature is of the order of 40 eV. In order to diagnose the propagation of the fast electrons in the bulk of the target, the Ti K-alpha line at 4.5 keV of embedded 20 µm thick Ti layers in Al/Ti/Al sandwich targets was imaged using a spherical Bragg crystal with a resolution of 10 µm. Two examples are shown in figure 3 (right). In agreement with XUV images taken in similar shots, the data show a minimum radius of 34 µm and a cone angle of ± 27°.

THEORETICAL AND NUMERICAL ACTIVITIES

In order to study fast electrons generation by ultra-intense laser pulses interacting with over-dense plasmas, 2D PIC simulations have been performed in various cases: sharp or smooth density gradients, weakly to strongly relativistic intensities, plane or focused waves.

In all cases, fast electrons are emitted with an angular spreading of their velocity, which cannot be explained by interface deformations or by the laser beam focusing.

It is found that, at least for sharp density gradients, this angular dispersion is linked to a transverse instability that is localized in the vicinity of the skin depth layer. High intensity magnetic fields are produced, leading to trapping and scattering of the energetic electrons. To illustrate these findings, the simulation of the interaction of a 10^{19} W/cm^2 laser pulse with a circular plasma - showing a linear density gradient from n_c (edge) to $5n_c$ (core) - is presented. The total radius of the target is 65 µm and the initial temperature is 10 keV.

One can see (figure 4) on the left image (the electron density being plotted) the onset of the formation of an asymmetrical, conical channel and the building of an over-dense electrostatic shock (black zone) in the exterior region of the target. In the right image (showing the electron energy), the asymmetry is also present in form of supra-thermal electron jets, preferentially bent toward the top of the image. A very fine structure, barely visible on this reduced image, is found at a wave number of 2 k_0^{-1}, suggesting an acceleration mechanism by the Lorentz force **jxB**. The observation of coherent transition radiation at the rear of laser-irradiated targets could be well related to these correlated electron jets, at twice the laser frequency, 2 ω_0.

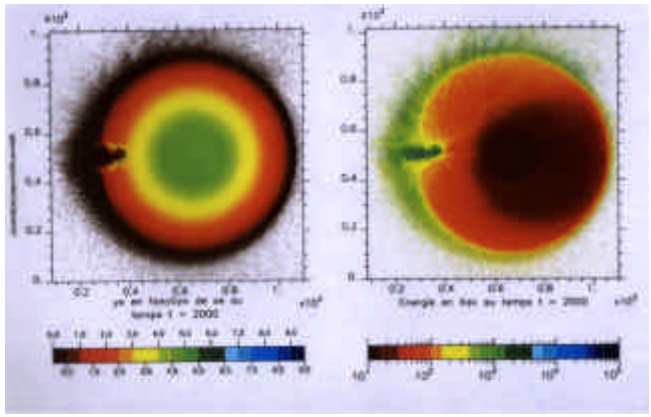

Figure 4 : Electron density (left) and electron energy (right, in keV) as a function of space at 1ps in the laser pulse (units are 1000 k_0^{-1}~160 µm)

The analysis of the electron currents is very instructive (see figure 5). Electrons of energies below 100 keV (left) make the return currents, oriented in the direction opposite to the laser.

Particle of intermediate energies (middle), penetrate deeply inside the target. The lack of mass currents in the target core is explained by the relatively lower electron temperature (as exhibited in figure 4 - right). The current asymmetry is clearly visible in the highest energy range (right).

Absorbed laser energy is about 20 % at 1ps into the laser pulse. This energy further increases with the continuing growth of the plasma channel.

In the field of positively charged particle acceleration, the freely expanding plasma model has been revisited in terms of charge separation effects and structure of the ion front.

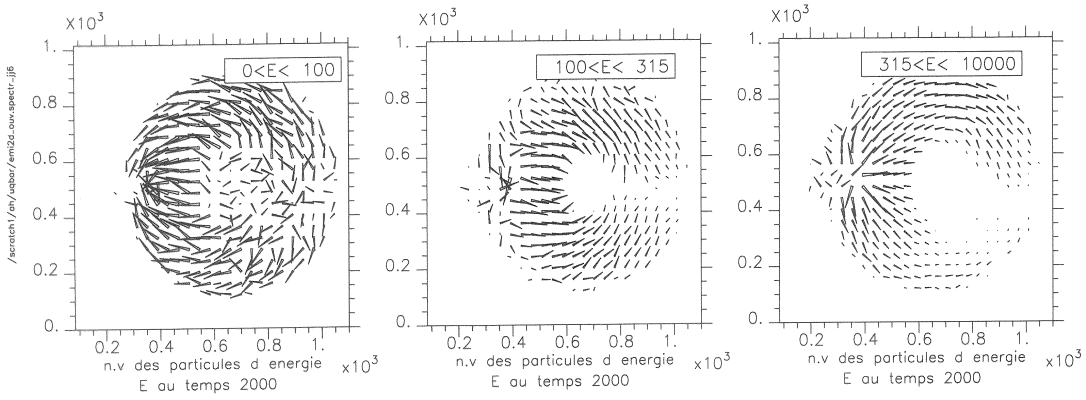

Figure 5 : Electron mass current maps at 1ps in the laser pulse for various ranges of electron energies (units are 1000 k_0^{-1} ~ 160 μm)

The 1D model solves the equations of continuity and motion for the ions, the charge separation field being obtained by the solution of the Poisson equation. The electrons obey a Boltzmann distribution at a given (supra-thermal, and even relativistic) temperature.

If one assumes quasi-neutrality, a self-similar solution of the model can be found, which is relevant to the physics of the ion acceleration mechanisms only if the initial Debye length is smaller than the self-similar scale length, governed by the (ion) speed of sound, i.e. for $\omega_{pi}t < 1$, where ω_{pi} is the ion plasma frequency. Otherwise, the self-similar model predicts an unrealistic infinite ion velocity.

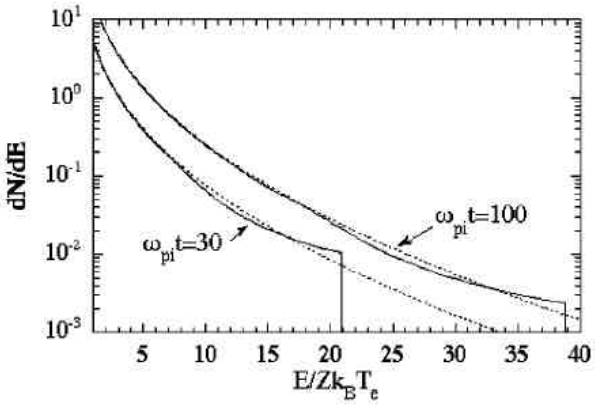

Figure 6 : Energy spectrum per surface unit for two different times in units of the plasma ion frequency, the dashed line being the self-similar solution

The numerical solution of the model provides much more physical results, as exemplified in figure 6.

The ion energy spectrum is plotted as a function of the ion scaled energy for two different times $\omega_{pi}t = 30$, and $\omega_{pi}t = 100$. Ions show a very well defined maximum energy evolving as the square of the logarithm of the scaled time $\omega_{pi}t$.

When comparing with real experiments, additional effects have to be taken into account, such as non-Maxwellian electron distributions, electron recirculation in thin foils, electron temperature dynamics, multi-dimensional effects, ionization mechanisms, and magnetic field effects.

CONCLUSIONS

Experiments on the generation and transport of fast electrons and on the resulting heating of the target have been conducted on the 100 TW LULI laser facility at a maximum intensity of □ 3 10^{19} W/cm^2 and a maximum laser energy of 10 J.

The results show a modest heating of the target, of the order of 20-40 eV up to 50 μm of Al.

This is consistent with about 10 % to 30 % of the laser energy being transferred to fast electrons inside a large angle cone, typically ± 20° to ± 40°.

2D PIC simulations have been performed for sharp or smooth density gradients, plane or focused waves.

In all cases, fast electrons are emitted with an angular spreading of their velocity, which cannot be explained by interface deformations or by the laser beam focusing.

High intensity magnetic fields are produced, leading to trapping and scattering of the energetic electrons. A simple model for ion (proton) acceleration based on free plasma expansion has been revisited.

Accurate results have been obtained concerning the structure of the ion front, the resultant ion energy spectrum, and more specifically the maximum ion energy.

REPORTS AND PUBLICATIONS

[1] O J. J. Santos, F. Amiranoff, S. D. Baton, L. Gremillet, M. Koenig, E. Martinolli, M. Rabec Le Gloahec, C. Rousseaux, D. Batani, A. Bernardinello, G. Greison, and T. Hall, Fast Electron Transport in Ultra intense Laser Pulse Interaction with Solid Targets by Rear-Side Self-Radiation Diagnostics, Physical Review Letters 89, 025001(2002).

[2] P. Mora, Plasma expansion into a vacuum, 6th Workshop on Fast ignition and relativistic plasma physics, Orlando, November 2002.

[3] J.C. Adam, A. Heron, G. Laval, and P. Mora, Angular dispersion of energetic electrons generated by the interaction ultraintense laser with an overdense plasma, 6th Workshop on Fast ignition and relativistic plasma physics, Orlando, November 2002.

TASK LEADER

Dr Arnold MIGUS

Laboratoire d'Utilisation des Lasers Intenses
Ecole Polytechnique
91128 Palaiseau

Tél. : 33 1 69 33 38 50 - 33 1 69 33 41 12
Fax : 33 1 69 33 30 09

E-mail : arnold.migus@polytechnique.fr

ICF04

Task Title: EU COLLABORATIVE EXPERIMENT ON THE FAST IGNITER CONCEPT

INTRODUCTION

Petawatt lasers are state-of-art tools to probe matter under the extreme conditions reached in Inertial Confinement Fusion. In order to simultaneously minimize their operation costs and maximize their performances (energy delivered on target, repetition rate), wave front analysis and control through active laser phase correction are of great importance.

The objective of this task is then to develop a complete automated system, consisting of an adaptative mirror and a phase front measurement device connected in a closed loop, to be inserted in the future LULI pico2000 and GSI PHELIX PW laser chains.

In a first exercise, prototype tests of the LULI closed-loop adaptive optics system (AOS), composed of a wave front sensor, a 98 mm bimorph deformable mirror and a Labview®-based convergence loop, have been conducted with cw-lasers. Then, the AOS has been implemented on the LULI 100TW laser facility and improvements of the beam focusability and of the repetition rate checked.

2002 ACTIVITIES

PROTOTYPE TESTS WITH CW LASERS

Description of the LULI adaptative optics closed-loop system (AOS)

Basically, an AOS is composed of three key elements:

- a wave front sensor: because of three remarkable properties: achromaticity, high resolution and adjustable sensitivity, an achromatic three-wave lateral shearing interferometer (ATWLSI) has been used;

- a deformable mirror: a 98 mm bimorph dielectric coated deformable mirror has been developed by the Adaptive Optics for Industrial & Medical Applications Group in Moscow and acquired by the LULI; 30+1 actuators allow theoretical correction up to Zernike 15^{th} order with excursions up to 6λ; the dielectric reflective coating meets the requirements for high damage threshold (> 3 GW/cm^{-2} in Δt = 1 ns);

- and a home-made Labview®-based convergence loop. A far-field measurement is systematically used to estimate the quality of the convergence.

Prototype tests

A large aperture (110 mm), high-quality, collimated beam issued from a cw YAG laser (λ = 1.06 μm) has been used for preliminary testing. Three points have been investigated: (a) calibration of the closed-loop system, (b) determination of the useful aperture comparing with the beam diameter, and (c) choice of a wave front reference. The results are the followings:

(a) a maximum phase shift of about 3λ and a rms of λ/1.32 is measured, when no voltage applied on the mirror; at the end of the convergence, the wave front distortion peak to peak decreases to 0.15λ and the rms to λ/50;

(b) 80% of the mirror aperture can be used for a good wave front correction;

(c) wave front reference can be generated using a pinhole located in the co-focal plane of an afocal system in front of the wave front sensor; the pinhole dimension is less than the diffraction limit.

IMPROVEMENT OF LULI 100TW CPA LASER SYSTEM FOCUSABILITY AND REPETITION RATE

Thermal effect evolution in the LULI 100 TW facility

The LULI 100TW CPA laser facility is composed of a 100 fs Ti:Sa oscillator, a temporal stretcher, a Ti:Sa regenerative pre-amplifier, a mixed Nd:glass amplification chain and a compressor. It delivers a 30 J/300 fs pulse on target, corresponding to the high peak power of 100 TW. The standard repetition rate of the facility for full-energy shots is 20 minutes. After each shot, the heat generated in the amplifiers by the flashlamp pumping system is responsible for most of the wave front distortion. This phase shift decreases towards zero only after 40 minutes.

In order to study the beam focusability of the LULI 100TW chain, a series of full-energy shots with the nominal repetition rate of 20 minutes have been carried. A far-field measurement is used to characterize the influence of the cumulative thermal effect.

The first shot is launched when the laser chain is cold, so that the focal spot exhibits a Strehl ratio of 0.8 with a full width at half maximum (FWHM) ~ 1.2 times diffraction-limited (figure 1(a)).

As full-energy shots are continuously launched every 20 minutes, the central peak spot becomes asymmetrical and larger and more energy is spread in large wings.

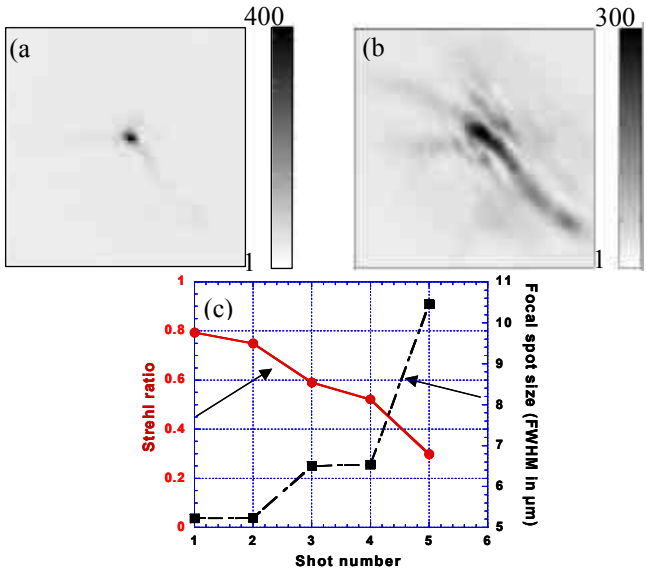

Figure 1 : Focusability of the LULI 100TW laser beam during a full-energy shot series (c) strong degradation of the 1st "cold" spot (a) is observed from the 5th shot (b)

Figure 1(b) shows the 5th shot strongly degraded focal spot. Along the shot sequence, the Strehl ratio (solid line on figure 1(c)) decreases from 0.8 to 0.3 and the central peak of the focal point (dashed line on figure 1(c)) stretches from 5 µm to more than 10 µm. In conclusion, wave front control and dynamic correction before each shot becomes mandatory if one wants to take advantage of the full repetition rate of 20 minutes while keeping a good focusability.

Closed-loop Adaptive Optics setup and wave front correction results

The closed-loop adaptative optics system has then been implemented on the LULI 100TW laser facility, and test during a series of full-energy. The 98 mm deformable mirror has been placed behind the 108 mm disk amplifier. 2 % of the total output energy is transmitted through the exit mirror and is used for wave front and far-field measurement.

Based on the wave front measurement à 10 Hz, the convergence loop and the phase correction are performed several seconds before each shot in order to avoid deviation of the phase.

The significant results can be summarized as follows:

- the near diffraction-limited focal spot recorded during the high-energy shot demonstrates the excellent focusability of the beam (see figure 4 (a));

- figures 4 (b) and (c) show a very good similarity of the focal spot between the first full-energy shot and the 5th shot. The near-diffraction-limited focal spot quality is maintained during this sequence of 20 minute full-energy shots with a calculated Strehl ratio 0.9.

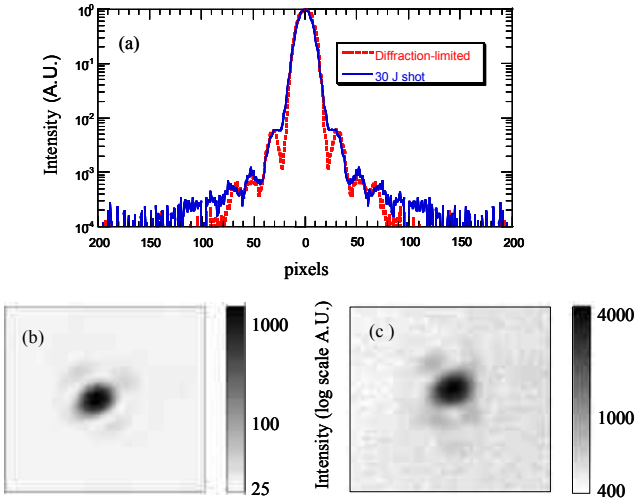

Figure 2 : Focusability of the LULI 100TW laser beam during a full-energy shot series if AOS operational: no degradation between the 1st "cold" spot (b) and the 5th shot (c) is observed; near-diffraction limited focalization is in fact reached (a)

CONCLUSIONS

These preliminary experiments have demonstrated that the precise measurement of the spatial phase distortion of a laser beam is essential to correctly design an AOS, especially to determine the actuator number and the actuator distribution for the deformable mirror. This will be shortly done on the currently under construction LULI kJ chain to finalize the PW concept.

REPORTS AND PUBLICATIONS

[1] J.P. Zou, J. Fuchs, B. Wattellier, J.C. Chanteloup, C. Haefner*, Improvement of the LULI high-energy CPA laser system focusability and repetition rate using an adaptive optical system, SPIE Proc., LAT2002 Moscou.

*GSI Darmstadt, Germany

TASK LEADER

Dr Arnold MIGUS

Laboratoire d'Utilisation des Lasers Intenses
Ecole Polytechnique
91128 Palaiseau

Tél. : 33 1 69 33 38 50 - 33 1 69 33 41 12
Fax : 33 1 69 33 30 09

E-mail : arnold.migus@polytechnique.fr

ICF-KiT-PRC

Task Title: OVERVIEW ON POWER REACTOR CONCEPTS

INTRODUCTION

The IFE-KiT task, for the FY2002 aimed at monitoring the worldwide progress in the Inertial Fusion Energy programs. It completes the last year monitoring assessment, [P1]. The details of this monitoring assessment are reported in [P2]. We expose here only the most marked progress. The most significant and relevant R&D activities are those carried out in the US research centers and universities, [P2]. We give in the following a brief description of the most marked progress in the IFE research activities.

2002 ACTIVITIES

PROGRESS IN IFE R&D ACTIVITIES

Although NIF, LMJ, GEKKO XII, SGII will provide the needed data on burning ICF & IFE plasma, none of them will have the capability to operate at high repetition rate nor to manage the fusion power at high repetition rate. Moreover, they have neither the efficiency nor the durability needed for the commercial power generation. Substantial scientific and technical issues must be identified, studied and resolved in parallel. The modularity of the IFE power plant components makes it possible to study these issues in scaled facilities where limited sub-sets of phenomena could be studied. That will guide the design and the construction of other experiments with higher level of integration.

The IFE community refers to these facilities as "Integrated Research Experiment" facilities or shortly IRE's facilities. This is one of the most significant achievements in the past recent years. The IRE's facilities should provide the bases of the sciences and technologies needed for the demonstration of the feasibility of the IFE power plants. Among these identified scientific and technical issues, the first wall of the IFE power plant attracts the highest interest.

The most significant efforts are those employed in the Liquid First Walls (thick, thin) research activities. Experiments with water jets, scaled to be hydro-dynamically equivalent to a power plant liquid chamber can now achieve both the required smooth jets and the principle of oscillation for rapid clearing after the shot [R1].

During 2001-2002, the IFE community has almost converged towards the "Nominal Baseline Power Plant Concepts", [P2]. This is indeed another significant achievement. It should allow in the next years to elaborate relevant R&D programs and to determine the "Requirements & Specifications for the IFE Power Reactor Concepts".

Other principal achievements, monitored in the US Fusion Community are:

- A consensual principal strategy for chamber R&D during the IRE phase founded on " … the development of detailed, integrated chamber response models." That includes both experimental and numerical models, [R2].

- The HIF power plant conceptual design that meets the pulse rate, cost, and efficiency and is consistent with the HIF requirements: the target beam energy, peak power, pulse shape, ion range, and focal spot size and which is consistent with a thick-liquid protected chamber, target illumination geometry, and propagation through hot chamber vapor [R2, Appendix I-HIF].

- A formal definition of the critical issues related to the base-line conceptual design for Heavy-Ion drivers uses thick-liquid chamber with indirect-drive, such as, [R2].

PROGRESS ON POWER REACTOR CONCEPTS DESIGN

An IFE Power Plant concept is the integrated design of a target, a driver, a chamber and a thermal power conversion system. As far as we are focusing on IFE Chamber concepts, three major categories are explored since the early age of investigations (~ 1980) and still being explored: dry-wall, wetted-wall and thick-wall designs. The concepts that are most mentioned in literature are given in [P2]. No significant progress has been monitored during the FY1999-2002.

All of these concepts have almost received relatively equal interest of the designers but are still at different state of progress and reporting. If we use as criteria the number of available papers and presentations on the concept in the scientific media, HILIFE-II and Sombrero are by so far the most referenced concepts (class 4).

They are followed by Osiris and Prometheus (class 3). Libra and Solase concepts occupy the 3rd rang (class 2). The least published is Hiball (class 1), [P2]. This classification counts only for the number of papers and presentations treating one or more aspects of the associated concept, where:

- Class 1: less than 5 published papers/presentations,

- Class 2: $5 <$ Nb of published papers/presentations ≤ 20,

- Class 3: $20 <$ Nb of published papers/presentations ≤ 40,

- Class 4: $40 <$ Nb of published papers/presentations.

It does not tell how original is the paper/presentation. Consequently, it does not reflect the new progress in the concept design. It is also limited to the papers/presentations monitored by the author.

This is almost the same situation since 1999, [R3], when the final report of the Inertial Fusion Concepts working group cites that: " The IFE power plant concepts thus appear to be settling down to two main lines;1) a heavy-ion, indirect drive target and a thick-wall chamber, and 2) a laser, direct drive target and a dry-wall chamber, both with a wetted-wall chamber as a "back-up" option". During the FY2002, this tendency has been confirmed.

REFERENCES

[R1] P. Peterson, "Inertial Fusion Technology (IT): the Science Basis for IFE Chambers and Targets" presentation to the Snowmass Fusion Summer Study, July 8, 2002.

[R2] "Snowmass Fusion Summer Study – Draft Report" Record Copy, Section 4.0.0.0 IFE Next Steps, revision B, Snowmass Summer Study workshop, 8-19 July, 2002, Snowmass, Colorado, USA.

[R3] "Snowmass Fusion Summer Study, July, 11-23, 1999, Final Reports of Working Groups." Draft (personal communication).

REPORTS AND PUBLICATIONS

[P1] M. Eid, "Assessment of the state-of-the-art of inertial fusion power reactor conceptual designs & associated technical risks." CEA report, DEN/DM2S, SERMA/LCA/01-2998/A, 11/2001.

[P2] M. Eid , "Inertial Fusion Energy: Monitoring of Worldwide R&D Activities, (1999-2002)." CEA report, DEN/DM2S, SERMA/LCA/RT/ 02-3187, 10/2002.

TASK LEADER

Dr. Mohamed EID

DEN/DM2S/SERMA
CEA Saclay
91191 Gif-sur-Yvette Cedex

Tél. : 33 1 69 08 31 75
Fax : 33 1 69 08 99 35

E-mail : mohamed.eid@cea.fr

ICF-XUV-Diag

Task Title: DENSE PLASMA DIAGNOSTICS USING HIGH ORDER HARMONICS GENERATION

INTRODUCTION

As well known, a laser pulse cannot propagate in a plasma whose density exceeds the corresponding critical density, N_c. For example, $N_c \approx 2.10^{21} e^-/cm^3$ for a wavelength of 790 nm. Thus, probing dense plasmas requires the use of short wavelength. The high order harmonics generated in rare gases [1], [2] provide such a source. They are spatially and temporally coherent, shorter than the initial pulse, naturally synchronised with the laser and can work at high repetition rate. For example, the 11th harmonic of the Ti-Sa laser, (λ = 72 nm) can propagate in a 10^{23} cm^{-3} density plasma over a distance of a fraction of micron. The attenuation of the harmonic comes from the very efficient linear absorption of the UV light by the plasma. In our experiments, the plasma is produced by intense irradiation of thin aluminium (Al) and plastic foils (100-200 nm thickness).

To create a hot, very far from equilibrium plasma, we focused a very intense and short laser pulse on the target. The intensity reached in the focus is close to $10^{18} W/cm^2$. We studied the temporal evolution of such a foil explosion. The way the plasma expands is supposed to give decisive information on the dynamics of the processes involved and on the existence of laser coupling conditions good enough to generate very high intensity effects such as hole boring creation, subject of interest for ignition fusion experiments.

We will report on two sets of experiments concerning the time dependant absorption of high order harmonics. These series of experiments will serve to prepare more ambitious studies which consist in interferometric measurements, allowing to evaluate the instantaneous refractive index and the electron temperature.

2002 ACTIVITIES

EXPERIMENTAL SET-UP

The experimental set-up is presented in figure 1. The UHI10 laser facility delivers 790 nm wavelength pulses (Ti:Sa laser based on the CPA technique) with 65 fs duration, at a repetition rate of 10 Hz. The energy per laser pulse is around 600 mJ, leading to a power of 10 TW. The system is divided in two parts: a low energy arm, with the same duration as the main pulse, is used to produce harmonics after focusing in a Xenon gas jet, and the ultra-intense arm is focused at 11.5° from the normal incidence on the target using a f = 50 cm off-axis parabolic mirror. The intensity at the focal point is close to 10^{18} W/cm^2.

The harmonics, focused on the thin film using a toroidal mirror without wavelength selection, are dispersed in a VUV spectrometer and detected on microchannel plates (MCP) coupled to a phosphor screen and a charge-coupled device (CCD) camera.

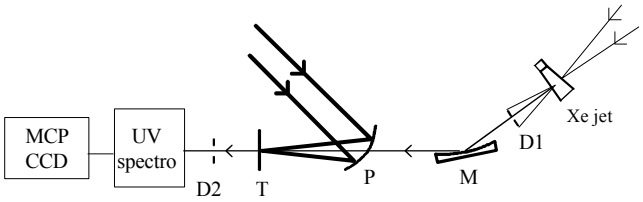

M : Toroidal focusing mirror
P : Off-axis holed parabolic mirror
T : Target (thin foils)
D1 : IR filtering diaphragm
D2 : diaphragm

IR pump beam
IR probe beam (annular)
High order Harmonics probe beam

Figure 1: Experimental set-up

EXPERIMENTAL RESULTS

First set of experiments

We limited the study to H_{11} in this run. In principle, the transmission of H_{11} (72 nm) in the 100 nm aluminium thin foil is of 65 % [3]. It was measured to be 20 %, resulting from the attenuation of the pure Al 100 nm foil and the additional oxidation (Al_2O_3) of the surface. This value is obtained by the evaluation of the ratio of the integrated signal recorded on the CCD camera when the harmonics pass through the target (in the case of Al foil) to the signal without any target. Note that we are sensitive to shot to shot fluctuations of the laser pulse generating the harmonics. This gives an error bar in any detected signal which has been evaluated to +/-10 %.

In figure 2, we present a temporal variation over 300 ps of the transmitted signal (normalised to the transmission of the Al foil without pump) recorded for the H_{11}. It shows clearly three features: for negative delays (the probe impinges the target before the main 10^{17} W/cm^2 pulse), the transmission is constant, in the vicinity of the peak intensity, the transmission varies very suddenly and latter, the transmission reaches a constant value. We note that, for negative delays, the transmission is about 40 % instead of the 20 % measured *without* pump. Close to the peak intensity, as shown in the inset of figure 2, the signal has a more complex time dependence. This behaviour was reproducible for many series: on the picosecond time scale, the transmission increases, then decreases and finally increases continuously to reach the final value of about 65 %.

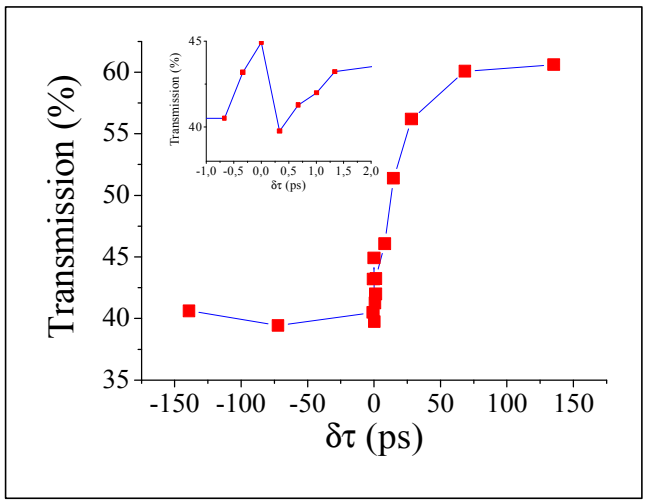

Figure 2 : Temporal evolution of the absolute transmission of H_{11} through a plasma created by irradiation ($I \approx 2.10^{17}$ W/cm²) of 100 nm Al foil, for a time delay (dt) between the pump and the probe pulse from –150 ps to +150 ps. Inset : zoom around the peak intensity

Second set of experiments

In this campaign, performed slightly after the previous one, three harmonics were detected simultaneously: H_{11}, H_{13}, H_{15}. The idea was that several harmonics (at least two) are expected to present different behaviours, giving the possibility to get simultaneously the plasma density and temperature [4]. A typical spectrum showing the three harmonics and the plasma self emission is presented in figure 3. The contrast between the harmonics signal and the plasma self emission was sufficiently high to detect intensity variation of harmonics.

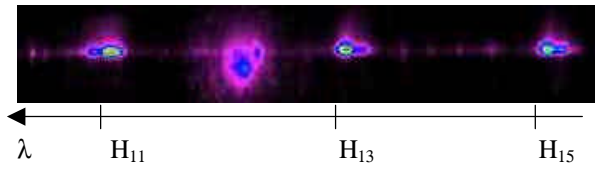

Figure 3 : Typical image of harmonics: H_{11}, H_{13} and H_{15} in presence of the high intensity pulse. The self emission of the plasma can be visualised all over the image, as well as an additional "ghost" signal located between the H_{11} and H_{13} signals

On figure 4, the results presented have been obtained with 100 nm Al foil. The temporal scale has been slightly reduced from -75 to +15 ps after the interaction with the pump laser pulse. We note that, if the general behaviour is at first sight not very different than previously, the error bar on the measurements is much more important than the one estimated coming from shot to shot fluctuations. In particular, the transmission close to the peak intensity presents a chaotic behaviour and is not, as it was before, reproducible.

To try to understand this new and unexpected situation, we changed the target to a 200 nm thickness plastic (C-H) foil. The difference is that the plastic cannot transmit harmonics. We are then supposed to start from an absence of transmission for negative delays.

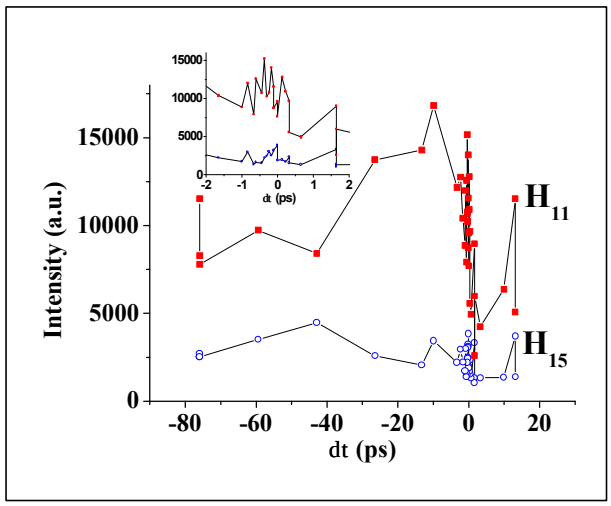

Figure 4 : Temporal evolution of the relative transmission of H_{11} through a plasma generated by irradiation ($I = 8{,}7.10^{17}$ W/cm²) of a 100 nm Al foil and a time delay (dt) from –75 ps to +15 ps Inset : zoom around the peak intensity

As shown in figure 5, it depends on the laser shot. Everything behaves as if sometimes the transmission is zero and sometimes not. As usual we observe an increase close to the maximum and, contrary to the metallic case, the transmission goes back to zero.

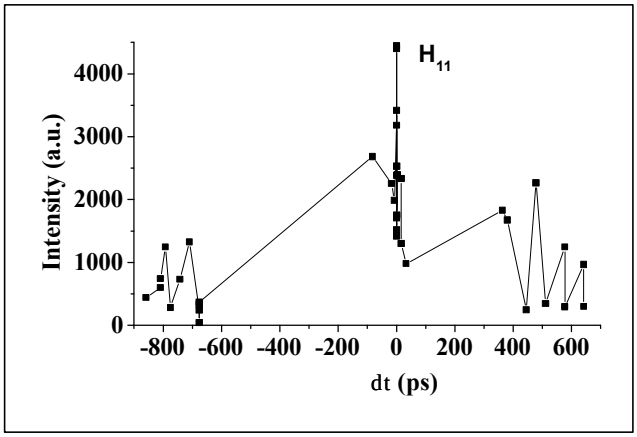

Figure 5 : Temporal evolution of the relative transmission of H_{11} through a plasma created by irradiation ($I = 3{,}2.10^{17}$ W/cm²) of 200 nm plastic foil for dt from –850 ps to 650 ps

DISCUSSION

Let us first discuss the results of the first set. The fact that the transmission is about 40 % instead of the 20 % measured *without* pump leads us to conclude that the signal is strongly influenced by the pedestal present in the pulse on nanosecond time scale, generating a plasma still in expansion well before the main peak.

We must then consider the propagation of a high intensity pulse in a relatively low density plasma [5]. Close to the maximum, the sudden increase and decrease of the transmission could be due to a hole boring effect (instantaneous channel creation by the main pulse) followed by a space charge repealing effect [6].

For long delays, the plasma temperature decreases leading, as well known, to an increase of the transmission.

The second set was supposed to confirm the previous results. That was not the case and that illustrates the sensitivity of this kind of experiments to the spatial and temporal laser profiles. This is confirmed with the experiment on C-H. Probing before the interaction with the main pulse have shown, with an amount of the shots, that the harmonics were not transmitted (unbroken foil) and with the rest that the harmonics were slightly transmitted (broken foil). It seems to show that we are submitted to the ASE and pre-pulses level variations which could play a crucial role in our experiment. This increases our error bar and makes difficult the interpretation of the results.

We can note that our diagnostic is better adapted to detect radial effects than longitudinal ones because the transmitted signal results from attenuation over the path length almost perpendicular to the target.

CONCLUSION AND SHORT TERM PERSPECTIVES

In this task, at the middle term of the first deliverable, we have pointed the major problem of the stability of the high intensity laser and especially the pedestal effects.

As the peak intensity of laser increases, the problem of the ratio between the main pulse and the prepulses and ASE energy becomes more and more crucial. In the same experiment, a part of the shots leads to the interaction of a high intensity pulse with a thin foil and for the other part of shots, the main pulse interacts with a pre-plasma. A pre-plasma is formed leading to laser energy absorption and propagation problems hard to control. We demonstrate that theses effects strongly penalise experiments where the direct interaction with the solid density is required. One of the possibilities to overcome this difficulty could be the use of the so called “plasma mirror” [7].

Briefly, the idea is to install before the target a transparent dielectric. Under suitable conditions, the dielectric remains transparent for the incident pedestal whereas the main peak is totally reflected. The rapid increase of reflectivity results from the interaction with the main pulse leading to sudden injection, by multiphotonic or tunnel ionisation, of enough electrons in the conduction band to overtake the critical density (2.10^{21} cm^{-3} at 790 nm). It is then reflected back without prepulses and ASE energy.

To conclude, after an adaptation of a more suitable geometry and a plasma mirror implementation, we have good confidence that our results concerning the transmission of harmonics will be reproducible. This is of prime importance for the continuation of this program in view of the interferometric measurements in the UV part of the spectra.

REFERENCES

[1] A. McPherson *et al* J. Opt. Soc. Am. B 4, 595 (1987).

[2] M. Ferray, A *et al*, J. Phys. B 21, L31 (1988).

[3] Tables of optical constants : http://cindy.lbl.gov.

[4] W. Theobald *et al*, Phys.Rev.E 59, 3554 (1999).

[5] K.B. Wharton *et al*, Phys.Rev.E 64, R025401 (2001).

[6] J. Fuchs *et al*, Phys.Rev.Lett 80, 1658 (1998).

[7] P. Audebert *et al*, to be submitted at Phys.Rev.E.

TASK LEADER

Ph. Martin

DSM/DRECAM/SPAM
CEA Saclay
91191 Gif-sur-Yvette Cedex

Tél. : 33 1 69 08 43 74
Fax : 33 1 69 08 9935

E-mail : martin@drecam.fr